Tissue Factor Pathway Inhibitor Overexpression Inhibits Hypoxia-Induced Pulmonary Hypertension

Thomas A. White[1], Tyra A. Witt[1], Shuchong Pan[1], Cheryl S. Mueske[1], Laurel S. Kleppe[1], Eric W. Holroyd[1], Hunter C. Champion[2]*, and Robert D. Simari[1]

[1]Mayo Clinic Division of Cardiovascular Diseases, Rochester, Minnesota; and [2]Johns Hopkins University, Baltimore, Maryland

Pulmonary hypertension (PH) is a commonly recognized complication of chronic respiratory disease. Enhanced vasoconstriction, pulmonary vascular remodeling, and *in situ* thrombosis contribute to the increased pulmonary vascular resistance observed in PH associated with hypoxic lung disease. The tissue factor pathway regulates fibrin deposition in response to acute and chronic vascular injury. We hypothesized that inhibition of the tissue factor pathway would result in attenuation of pathophysiologic parameters typically associated with hypoxia-induced PH. We tested this hypothesis using a chronic hypoxia–induced murine model of PH using mice that overexpress tissue factor pathway inhibitor (TFPI) via the smooth muscle–specific promoter SM22 (TFPI^{SM22}). TFPI^{SM22} mice have increased pulmonary TFPI expression compared with wild-type (WT) mice. In WT mice, exposure to chronic hypoxia (28 d at 10% O_2) resulted in increased systolic right ventricular and mean pulmonary arterial pressures, changes that were significantly reduced in TFPI^{SM22} mice. Chronic hypoxia also resulted in significant pulmonary vascular muscularization in WT mice, which was significantly reduced in TFPI^{SM22} mice. Given the pleiotropic effects of TFPI, autocrine and paracrine mechanisms for these hemodynamic effects were considered. TFPI^{SM22} mice had less pulmonary fibrin deposition than WT mice at 3 days after exposure to hypoxia, which is consistent with the antithrombotic effects of TFPI. Additionally, TFPI^{SM22} mice had a significant reduction in the number of proliferating (proliferating cell nuclear antigen positive) pulmonary vascular smooth muscle cells compared with WT mice, which is consistent with *in vitro* findings. These findings demonstrate that overexpression of TFPI results in improved hemodynamic performance and reduced pulmonary vascular remodeling in a murine model of hypoxia-induced PH. This improvement is in part due to the autocrine and paracrine effects of TFPI overexpression.

Keywords: pulmonary hypertension; tissue factor; tissue factor pathway inhibitor; hypoxia

CLINICAL RELEVANCE

This research focuses on the mechanisms by which tissue factor pathway inhibitor overexpression attenuates many of the detrimental pathophysiologic changes that occur in a hypoxia-induced murine model of pulmonary hypertension. Data derived from this study suggest that inhibition of the tissue factor pathway may be a potential novel approach for the treatment of pulmonary hypertension associated with hypoxic lung disease.

Pulmonary hypertension (PH) is a commonly recognized complication of chronic respiratory disease (1). PH due to disorders of the respiratory system or hypoxemia is recognized as an established entity by the World Health Organization and includes PH due to interstitial lung disease, chronic obstructive pulmonary disease, sleep-disordered breathing, alveolar hypoventilation disorders, and other causes of hypoxemia (2). PH in patients with hypoxic lung disease is associated with increased morbidity and reduced survival (3–6). Sustained pulmonary hypoxia induces a progressive and sustained increase in pulmonary vascular resistance, leading to an increase in pulmonary arterial pressure and, if left untreated, right ventricular failure and death. Enhanced vasoconstriction, pulmonary vascular remodeling, and *in situ* thrombosis contribute to the increased pulmonary vascular resistance observed in PH associated with hypoxic lung disease (7, 8). The pulmonary vascular remodeling associated with hypoxia-induced PH is characterized by intimal thickening and fibrosis, medial hypertrophy, muscularization of previously nonmuscularized arteries, adventitial proliferation, and abnormal extracellular matrix deposition (9–14).

Tissue factor (TF) is a procoagulant glycoprotein that triggers the extrinsic coagulation cascade. Activation of the TF pathway leads to the generation of thrombin, which catalyzes the conversion of fibrinogen to fibrin. TF has also been shown to stimulate vascular cell migration and proliferation independent of its procoagulant activity (15, 16). Tissue factor pathway inhibitor (TFPI) is the major physiologic inhibitor of the TF pathway (17–20). TFPI has also been shown to inhibit vascular smooth muscle cell (SMC) migration and proliferation and endothelial cell proliferation through mechanisms independent of its anticoagulant activity (21–23). Several studies have demonstrated that patients with PH have enhanced procoagulant and decreased fibrinolytic function of the pulmonary endothelium resulting in a prothrombotic or hypercoagulable state (24, 25).

Multiple lines of evidence suggest that the TF pathway may be involved in the pathogenesis of PH. In humans, increased pulmonary expression of TF, an increase in TF-bearing microparticles, and a decrease in circulating forms of TFPI have been noted (26, 27). TF is also expressed in pulmonary plexiform-like lesions in humans and in a rat model of severe pulmonary hypertension (28, 29). Furthermore, chronic hypoxia elicits pulmonary vasoconstriction and pulmonary vascular remodeling in mice (30). TF expression is strongly induced by hypoxic conditions, which promotes pulmonary fibrin deposition and pulmonary vascular thrombosis (31–34).

Taken together, these data suggest that increased TF expression or decreased TFPI expression may predispose patients with PH to *in situ* thrombosis, which may explain the pulmonary vascular thrombosis frequently observed in these patients. We therefore hypothesize that the tissue factor pathway may play a critical role in the development and progression of hypoxia-

(*Received in original form April 27, 2009 and in final form July 15, 2009*)

This work was supported by National Heart, Lung and Blood Institute grant HL65191 (R.D.S.).

* Present affiliation: University of Pittsburgh Medical Center, Pittsburgh, Pennsylvania.

Correspondence and requests for reprints should be addressed to Robert D. Simari, M.D., Mayo Clinic Division of Cardiovascular Diseases, Rochester, MN 55905. E-mail: simari.robert@mayo.edu

Am J Respir Cell Mol Biol Vol 43. pp 35–45, 2010
Originally Published in Press as DOI: 10.1165/rcmb.2009-0144OC on July 31, 2009
Internet address: www.atsjournals.org

induced PH. In the present study, we examined the effects of TFPI overexpression on hemodynamic parameters, pulmonary fibrin deposition, and pulmonary vascular remodeling in a murine model of hypoxia-induced PH.

MATERIALS AND METHODS

All experimental procedures and protocols used in this investigation were reviewed and approved by the Institutional Animal Care and Use Committees of the Mayo Clinic and Johns Hopkins. Handling of all mice conformed to the National Institutes of Health and the Mayo Clinic College of Medicine institutional guidelines.

TFPI^{SM22} Mice

Transgenic mice (TFPI^{SM22}) that overexpress TFPI via the smooth muscle–specific promoter SM22 have been described previously (35). These mice were generated and have been maintained on a C57/Bl6 background. Age-matched C57/Bl6 mice (wild-type [WT]) were used as controls in all experiments. Male mice (~12–16 wk of age) were used in all experiments.

Transgene Expression

The transgene was designed to contain a human-myc tag. We used this fact to design primers specific for the transgene (TFPI-myc) and to examine transgene expression in WT and TFPI^{SM22} mice. We also examined SM22 expression in tissue from WT and TFPI^{SM22} mice. RNA was extracted from 20 to 30 mg of lung and whole aortas using an RNeasy Plus Mini Kit (Qiagen, Inc., Valencia, CA) per the manufacturer's protocol. This method results in the purification of high-quality RNA, with good yield and no detectable genomic DNA contamination. First-strand cDNA synthesis was performed using SuperScript First-Strand Synthesis System for RT-PCR (Invitrogen, Carlsbad, CA) per the manufacturer's protocol. PCR was then performed, products were separated on 2% agarose gels containing ethidium bromide, and products were visualized by UV transillumination. The following primers were used: TFPI-myc forward, CCC AGTGAATGAGGTACA; TFPI-myc reverse, TTCTGAGATGAGT TTTTGTTC; SM22 forward, GCCCAGACACCGAAGCTA; SM22 reverse CTGCTGCCATATCCTTACCTT.

Real-Time PCR

We examined the effects of transgene expression on pulmonary TFPI expression in WT and TFPI^{SM22} mice. TF expression was also examined. A 20- to 30-mg piece of lung was homogenized, and total RNA was extracted using an Rneasy Plus Mini Kit (Qiagen). First-strand cDNA synthesis was performed using SuperScript First-Strand Synthesis System for RT-PCR (Invitrogen). Expression of pulmonary TF and TFPI was examined by real-time PCR using a LightCycler 480 instrument (Roche Applied Science, Indianapolis, IN) and hydrolysis probe (Universal ProbeLibrary, Roche Applied Science) technologies. Primers and hydrolysis probes specific for a gene transcript of interest allows the specific relative quantification of gene expression. Beta-actin (ACTB) was used as a "housekeeping" gene, and a reference gene set was used to normalize expression levels of TF and TFPI. The following primer probe sets were used: mouse TF, forward primer GAGACG GAGACCAACTTGTGA, reverse primer GGCTGTCCGAGGTTT GTG, Universal Probe #52; mouse TFPI, forward primer TGCAAG AAGATCTGTGAGAATCC, reverse primer ACGTAGTCACTCAT CTGTACCTCATT, Universal Probe #60. For mouse ACTB, primer and probe sets were contained in a Universal ProbeLibrary Mouse ACTB Gene Assay set (Roche).

Western Blot Analysis of Pulmonary TFPI and TF

Lung tissue was finely minced using a razor blade in a petri dish on ice and transferred to a microcentrifuge tube using 1 ml PBS. Minced tissue was centrifuged at 12,000 × *g* for 5 minutes at 4°C. The supernatant was discarded, and the tissue pellet was homogenized in lysis buffer consisting of PBS containing 30 mM CHAPS, 10 μM E-64, 1 mM PMSF, and 10 mM EDTA. The resulting homogenates were incubated on ice for 30 minutes followed by centrifugation at 12,000 × *g* for 10 minutes at 4°C. The supernatants were transferred to new tubes and frozen at −80°C until analysis. The protein concentration of each homogenate was determined using the colorimetric Bio-Rad *DC* Protein Assay (Bio-Rad, Hercules, CA) by extrapolation to a standard curve using BSA as standard. Samples were then subjected to SDS-PAGE using 10% acrylamide gels under reducing conditions and transferred to PVDF membranes. The blots were blocked in Tris-buffered saline/0.05% Tween-20 (TBST) containing 5% nonfat dry milk for 1 hour at 20°C and subsequently incubated with primary antibodies to TFPI, TF (Santa Cruz Biotechnology, Santa Cruz, CA), or β-actin (Abcam Inc., Cambridge, MA) at dilutions of 1:200 for TFPI and TF or 1:2,000 for β-actin in TBST with 5% nonfat dry milk overnight at 4°C. After washing in TBST (3 × 5 min), the blots were incubated with a 1:5,000 dilution of horseradish peroxidase–conjugated secondary goat anti-rabbit antibody (Santa Cruz Biotechnology) in TBST with 5% nonfat dry milk for 1 hour. Blots were washed three times for 5 minutes in TBST followed by a single 5-minute wash in Tris-buffered saline. Bands were visualized using SuperSignal West Pico Chemiluminescent Substrate (Pierce Biotechnology, Inc., Rockford, IL) and analyzed by densitometry. After each blot was analyzed, the membranes were stripped using Restore Western Blot Stripping Buffer (Pierce), reblocked, and reprobed with another primary antibody. This allowed each sample to be analyzed for TFPI, TF, and β-actin. Values for TFPI and TF were normalized to β-actin.

Hypoxic Induction of Pulmonary Arterial Hypertension

TFPI^{SM22} mice and WT mice were maintained under ambient air conditions (normoxic) or in a hypoxia chamber (ProOx and A-Chamber; BioSpherix, Redfield, NY) maintained at 10% O_2 (hypoxic) for a period of 0, 3, 7, or 28 days. Animals were fed standard mouse chow and were allowed access to food and water *ad libitum*.

Hemodynamic Measurements

After induction of anesthesia using isofluorane, animals were ventilated using a small rodent ventilator (MiniVent; Harvard Apparatus, Holliston, MA) through tracheal cannulation. Anesthesia was maintained using 1 to 2% isofluorane throughout the remainder of the experiment. A thoracotomy was performed and a 1.2 French pressure/volume catheter attached to a transducer (Scisense Inc., London, ON, Canada) was directly inserted into the right ventricular lumen and right ventricular pressures, and volumes were detected. The associated pressure/volume control box for the catheter contains signal acquisition and amplification circuitry, providing analog pressure and volume signals, which were collected via connection to a PC-driven PowerLab with ChartPro software (ADInstruments, Colorado Springs, CO). Waveforms were monitored during the procedure to ensure accurate measurements. Hemodynamic parameters were calculated using CardioSoft software (Sonometrix Corp., London, ON, Canada).

Assessment of Right Ventricular Hypertrophy

Hearts were perfused with 0.9% saline to remove residual blood, the right ventricle (RV) was dissected from the left ventricle (LV) plus septum. The RV and LV plus septum were weighed and the (RV)-to-(LV + septum) ratio was calculated as an index of right ventricular hypertrophy (36–38).

Assessment of Pulmonary Vascular Remodeling

The muscularization of pulmonary vessels was determined as described previously (36, 39). Pulmonary vessels with external diameters between 25 and 100 μm landmarked to an airway distal to the respiratory bronchiole were counted. Vessels were considered muscularized if a muscularized media was seen around the entire vessel. Vessels with a muscularized media that did not completely surround the vessel were considered partially muscularized, and those without any muscularized media were considered nonmuscularized. Percent muscularization of pulmonary vessels for each side examined was calculated as (number of muscularized and partly muscularized vessels)/total number of vessels counted × 100.

Immunohistochemistry

Lungs were perfused with 10% neutral buffered formalin and imbedded in paraffin. Fibrin(ogen) staining was obtained using 5-μm paraffin sections heated to 55°C and depariffinized with xylene and ethanol.

Antigen retrieval was performed using 10 mM citrate buffer (pH 6.0). The sections were blocked with 10% normal horse serum for 30 minutes, followed by an overnight incubation at 4°C with goat anti-mouse fibrinogen, (Accurate Chemical and Scientific Corp., Westbury, NY), diluted 1:500. This antibody recognizes both fibrin and fibrinogen. A negative control, replacing the primary antibody with goat IgG at the same concentration, was included. Biotinylated horse anti-goat, (Vector Laboratories, Burlingame, CA) diluted 1:200 was followed by an incubation with Alkaline Phosphatase Streptavidin. The reaction was visualized using Vector Blue. Quantification was performed using a microscope based video image analysis system (Image One Systems; Universal Imaging, West Chester, PA). Fibrin staining was analyzed in a blinded fashion on 20 high-power fields per lung section and expressed as percent fibrin staining per total area.

Measurement of Circulating TFPI and TF Activities

Immediately after the measurement of right ventricular pressures, 100 μl of blood was collected into a tube containing 10 μl sodium citrate and centrifuged at 10,000 × *g* for 10 minutes at 4°C, and the resulting plasma was transferred to new tubes and frozen at −80°C until analysis. Plasma TFPI activities were measured using an ACTICHROME TFPI Activity Assay kit (American Diagnostica Inc.) per the manufacturer's protocol. Plasma TF activities were measured using an AssaySense TF Chromogenic Activity Assay kit (Assaypro, St. Charles, MO) per the manufacturer's protocol.

TFPI ELISA Assay

Retro-orbital blood samples (100 μl) were obtained from C57BL/6 mice (8–12 wk) at 5, 15, or 60 minutes after tail vein heparin infusion (100 U heparin in 100 μl). Control (Baseline) mice were tail vein infused with saline instead of heparin. Blood was collected into 3.8% sodium citrate solution and plasma was separated by centrifugation (13,000 rpm, 10 min). TFPI ELISA assays were performed using the Protein Detector ELISA Kit (Kirkegaard and Perry Laboratories, Inc., Gaithersburg, MD) per manufacturer's protocol. In brief, 100 μl of plasma samples (diluted 1:500 in coating buffer) were incubated for 1 hour at room temperature and then removed from the 96-well ELISA plate. Blocking buffer was added to each well followed by incubation with purified rabbit anti-mouse TFPI polyclonal (1 μg/ml) antibody (diluted 1:50 into blocking buffer) for 1 hour at room temperature. The plate was washed five times, incubated with HRP conjugated anti-rabbit IgG antibody for 1 hour at room temperature, and washed again. Substrate solution was added and the plate was read at 405 nm. Media from HEK293 cells transfected with mouse TFPI was used as a positive control. Serial diluted recombinant mouse TFPI (kindly provided by Drs. Harold Roberts and Jen-yea Chang, University of North Carolina) was used to generate a standard curve.

Immunofluorescence Staining

For pulmonary localization of fibrin and von Willebrand factor (vWF), 5-μm paraffin sections heated to 55°C and depariffinized with xylene and ethanol. Antigen retrieval was performed using 10 mM citrate buffer, pH 6.0. Sections were subsequently blocked with 10% normal donkey serum (Sigma, St. Louis, MO) for 30 minutes and incubated overnight at 4°C with 20 μg/ml goat anti-mouse fibrinogen (Accurate Chemical and Scientific Corp.). Goat IgG (Sigma), same concentration, was used as the negative control. The sections were then incubated 45 minutes with donkey anti-goat AF488 (Molecular Probes, Eugene, OR) to visualize the fibrin. This was followed by blocking with 10% normal goat serum (Sigma) for 30 minutes and incubating 60 minutes at room temp with 15.5 μg/ml rabbit anti-human vWF (Dako, Carpinteria, CA) or rabbit IgG (R&D Systems, Minneapolis, MN) for control. This was visualized using goat anti-rabbit Texas Red (Molecular Probes). Nuclei were stained with Hoechst 33258 (Sigma).

For localization of proliferating cell nuclear antigen (PCNA) and α-actin, 5-μm sections were prepared as above and incubated for 30 minutes in 10 mM Tris buffer containing1 mM EDTA (pH 9.0) at 100°C for antigen retrieval. After blocking for 30 minutes with 10% normal goat serum (Sigma), the sections were incubated overnight at 4°C with 1 μg/ml rabbit anti-PCNA (Santa Cruz Biotechnology). Rabbit IgG (R&D Systems) at the same concentration was used as the negative control. The sections were next incubated for 30 minutes with biotinylated goat anti-rabbit IgG (Dako, Carpinteria, CA), followed by Alkaline Phosphatase Streptavidin (Vector Labs, Burlingame, CA), and visualized using Vector Red Alkaline Phosphatase Substrate Kit I (Vector Labs). This was followed by 15 minutes of blocking with 10% normal goat serum (Sigma) and incubating 60 minutes with 0.7 μg/ml mouse anti-human smooth muscle actin (Dako) or mouse IgG (R&D Systems) for control. This was visualized using goat anti-mouse FITC (Molecular Probes). Nuclei were stained with Hoechst 33258 (Sigma). Stained lung sections were assessed using a LSM 510 Confocal Laser Scanning Microscope (Carl Zeiss, Inc., Oberkochen, Germany). Two indexes of proliferation were calculated as follows: (*1*) total cell proliferation index = # of PCNA positive vascular cells/total # of vascular cells × 100 and (*2*) SMC proliferation index = number of PCNA-positive vascular SMCs divided by the total number of vascular SMCs × 100. Fifteen vessels (20–100 μm in diameter) per animal with three animals per group were analyzed in a blinded fashion.

Aortic SMC Isolation

Aortas were removed from mice and cleaned of adventitia under a dissecting microscope. Aortas from three mice were pooled and minced in ice-cold Dulbecco's modified PBS without Ca^{2+} or Mg^{2+} and transferred to a sterile 10-ml glass tube. Pieces of aorta were allowed to settle, the Dulbecco's modified PBS was removed and replaced with 5 ml of Hanks' balanced salt solution buffered with 20 mM HEPES (HBSS, pH 7.4) containing 0.25 mg/ml soybean trypsin inhibitor, 2 mg/ml BSA, and 2 mg/ml collagenase type I. The tube was placed on a rocking platform at 37°C for 45 minutes. The tissue was triturated vigorously to disperse endothelial as well as other loosely associated cells. The tissue pieces were allowed to settle and the supernatant containing dissociated cells was discarded and replaced with 5 ml of HBSS containing 0.25 mg/ml soybean trypsin inhibitor, 2 mg/ml BSA, 0.625 U/ml elastase and 10 mg/ml collagenase type I. The tube was again placed on a rocking platform at 37°C for 40 minutes. The tissue was triturated vigorously to disperse SMCs. Undigested pieces were allowed to settle and the cell suspension was filtered through a 100-μm cell strainer into a 50-ml conical tube. The strainer was rinsed with 10 ml smooth muscle growth medium (SmGM) (Lonza, Basel, Switzerland). The cells were pelleted by centrifugation at 300 × *g* for 5 minutes, resuspended in 10 ml SmGM and this centrifugation and resuspension was repeated an additional two times. The final cell pellet was resuspended in 1 ml SmGM and the entire suspension was seeded to a 75-cm^3 flask with an additional 15 ml SmGM. The cells were maintained in an incubator at 37°C with 5% CO_2. Medium was replaced the following day and then replaced every 3 to 4 days. Cells were confirmed to be SMCs by immunostaining for smooth muscle specific α-actin and SM22.

Proliferation Assay

At passage, aortic SMCs from WT or $TFPI^{SM22}$ mice were plated into a 96-well plate (5,000 cells per well). After 24 hours, SmGM was replaced with BrdU labeling solution (Roche Applied Science, Penzberg, Germany) consisting of a 1:100 dilution of BrdU labeling reagent in SmGM. Cells were cultured overnight in an incubator at 37°C with 5% CO_2. Incorporation of BrdU was then assayed according to the manufacturer's protocol.

Statistical Analysis

All results are expressed as means ± SEM. In all experiments, differences between control and treated groups were analyzed for statistical significance using a one-way ANOVA or an unpaired Student's *t* test (two-tailed). In the case of ANOVA, a multiple comparison test was used to compare all groups.

RESULTS

The SM22α Promoter Drives Pulmonary Transgene Expression

As previously described (35), we used a transgenic mouse in which murine TFPI (myc tagged) is expressed from the murine

SM22α promoter. To determine whether the transgene is expressed in the lungs of transgenic mice, we examined transgene and SM22α expression in tissue from WT and TFPI^{SM22} mice. Transgene expression was present in the lungs and aortas of TFPI^{SM22} mice and was absent in WT mice (Figure 1). SM22α mRNA was present in lung and aortic tissue from WT and TFPI^{SM22} mice (Figure 1). Real-time PCR analysis was used to quantify TFPI and TF expression in lung tissue. There was an approximate 3.6-fold increase in pulmonary TFPI mRNA expression in TFPI^{SM22} mice compared with WT mice, whereas TF mRNA expression was not significantly different between the groups of mice (Figure 2A). Western blot analysis also revealed a significant increase in pulmonary TFPI protein expression in TFPI^{SM22} mice when compared with WT mice (Figure 2B). TF protein expression in WT and TFPI^{SM22} mice was not different. These results demonstrate that SM22α-driven transgene expression results in a significant elevation of pulmonary TFPI expression without effecting TF expression.

Overexpression of TFPI Inhibits the Hemodynamic Response to Chronic Hypoxia

In normoxic conditions, there were no differences in pulmonary hemodynamics between WT and TFPI^{SM22} mice. WT mice exposed to hypoxia (10% O_2) for 28 days (WT hypoxic) had a 106% increase in right ventricular systolic pressure (RVSP) from 19.9 ± 0.5 mm Hg to 40.9 ± 0.8 mm Hg compared with WT normoxic mice (Figures 3A and 3B; $P < 0.001$). This increase in right ventricular pressure was only 52% in TFPI^{SM22} mice exposed to hypoxia compared with TFPI normoxic mice (from 22.1 ± 0.9 mm Hg to 33.6 ± 0.9 mm Hg) (Figures 3A and 3B). Similar changes were seen in pulmonary artery pressures (Figure 3C). Chronic hypoxia induced a 122% increase in mean pulmonary arterial pressure in WT mice (from 14.7 ± 0.2 to 32.6 ± 0.8 mm Hg). In TFPI^{SM22} mice this increase was significantly lower (from 14.9 ± 0.1 to 27.2 ± 1.5 mm Hg; 83%).

Hypoxia resulted in a significant decrease in cardiac output (from 13.2 ± 5 ml/min in WT normoxic mice to 9.3 ± 7 ml/min in WT hypoxic mice) but was maintained in TFPI^{SM22} mice (13.4 ± 8 ml/min for TFPI^{SM22} normoxic versus 14.0 ± 7 ml/min for TFPI^{SM22} hypoxic mice) (Figure 3D). Right ventricular ejection fraction was also significantly decreased (from 68.1 ± 2.4% in the WT normoxic mice to 39.2 ± 4.6% in the WT hypoxic mice), whereas in the TFPI^{SM22} normoxic and TFPI^{SM22} hypoxic mice there was no significant difference (69.2 ± 2.1% versus 60.5 ± 1.8%, respectively) (Figure 3E).

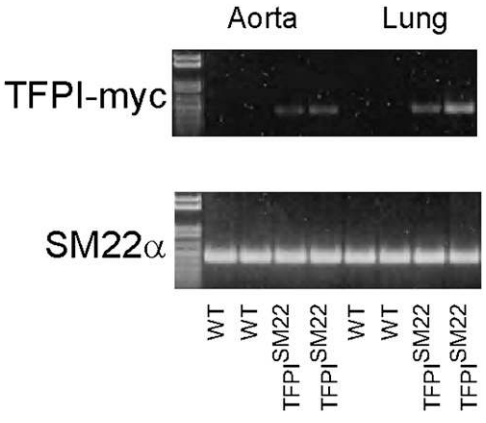

Figure 1. Tissue factor pathway inhibitor (TFPI)-myc transgene and SM22 expression. RT-PCR was performed on total RNA from aortas and lungs of wild-type (WT) mice or mice that overexpress TFPI via the smooth muscle specific promoter, SM22 (TFPI^{SM22}). TFPI-myc transgene expression was observed only in aorta and lung from TFPI^{SM22} mice, whereas SM22 expression is expressed in WT and TFPI^{SM22} mice.

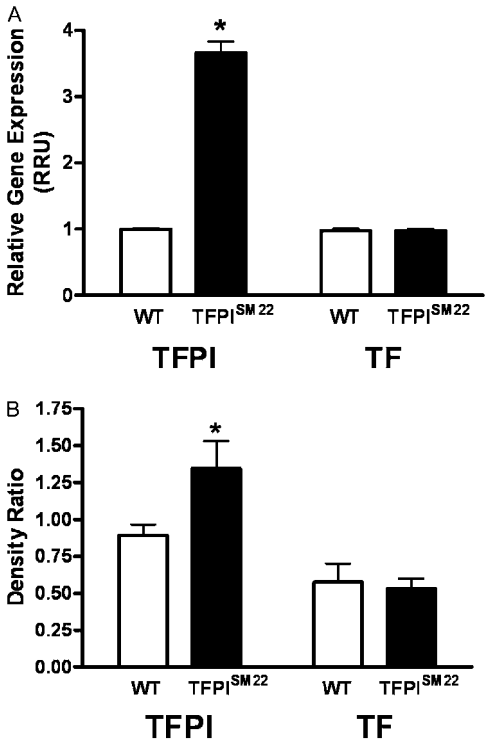

Figure 2. Analysis of pulmonary TFPI and tissue factor (TF) expression. (*A*) Real-time PCR was performed on total RNA extracted from lungs of WT ($n = 4$) mice or TFPI^{SM22} mice($n = 4$). A significant increase in pulmonary TFPI expression was observed in TFPI^{SM22} mice compared with WT mice (*$P < 0.0001$ compared with WT). There were no significant differences in TF expression. Relative RNA units (RRU) were normalized to β-actin levels and calculated from standard curves. (*B*) Western blot analysis was performed using lung lysates from WT ($n = 8$) and TFPI^{SM22} mice ($n = 8$). TFPI and TF were quantified by densitometry and normalized to β-actin. There is a significant increase in TFPI protein expression levels in TFPI^{SM22} mice compared with WT mice (*$P < 0.05$). There were no significant differences in TF protein expression.

Overexpression of TFPI Inhibits Cardiac Hypertrophy

WT and TFPI^{SM22} mice exposed to chronic hypoxia develop significant RV hypertrophy when compared with normoxic control mice as measured by the ratio of RV to LV and septal weights (Figure 4). Right ventricular hypertrophy was significantly reduced in the TFPI^{SM22} mice ($P < 0.05$). This ratio was 0.25 ± 0.01 in WT normoxic mice and increased to 0.39 ± 0.01 in the WT hypoxic mice, a 56% increase. The ratio was 0.26 ± 0.01 in TFPI^{SM22} normoxic mice and increased to 0.36 ± 0.01 in the TFPI^{SM22} hypoxic mice, a 38% increase.

Overexpression of TFPI Inhibits Pulmonary Vascular Remodeling

Pulmonary vascular remodeling including the muscularization of pulmonary vessels is an important feature of PH. Increased pulmonary vascular remodeling, as measured by an increase in the percentage of pulmonary vessels that are fully or partly muscularized, is evident in WT and TFPI^{SM22} hypoxic mice (Table 1). The percentage of fully muscularized vessels was

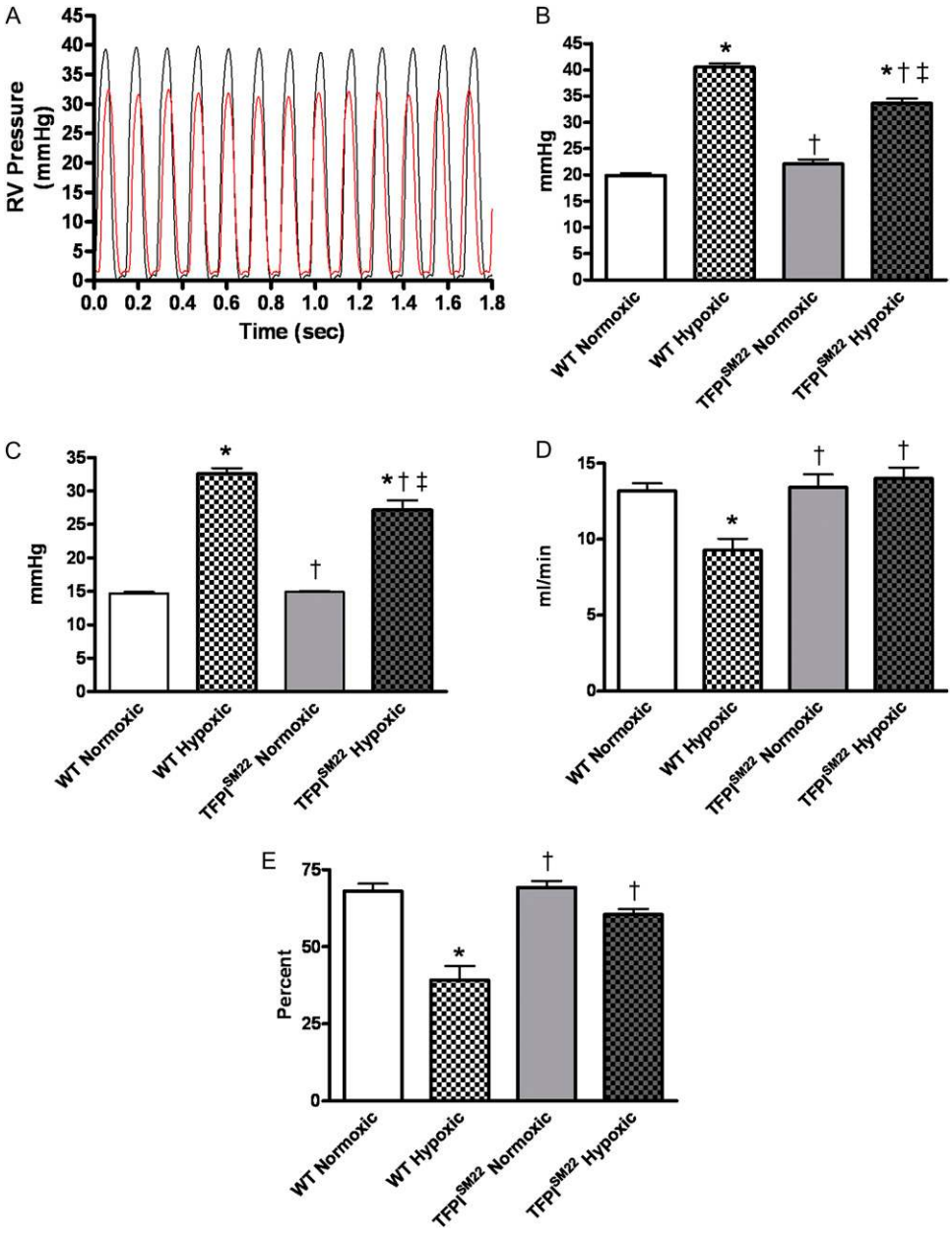

Figure 3. Effect of TFPI overexpression on hemodynamic parameters in hypoxia-induced pulmonary arterial hypertension. Hemodynamic parameters were assessed in WT mice or TFPI^{SM22} mice. Mice were maintained under normoxic conditions (normoxic) or exposed to 28 days of hypoxia (10% O_2, hypoxic). No differences in any parameters were observed between WT normoxic and TFPI^{SM22} normoxic mice. (*A*) Pressure tracings from a representative experiment showing a reduction in right ventricular systolic pressure (RVSP) in TFPI^{SM22} mice compared with WT hypoxic mice. (*B*) Significant increases in RVSP were observed in WT hypoxic and TFPI^{SM22} hypoxic mice. This increase was significantly attenuated in the TFPI^{SM22} hypoxic mice (*$P < 0.001$ compared with WT normoxic mice; †$P < 0.001$ compared with WT hypoxic mice, and ‡$P < 0.001$ compared with TFPI^{SM22} normoxic mice; n = 11–12 animals per group). (*C*) Mean pulmonary arterial pressures are increased in WT hypoxic and TFPI^{SM22} hypoxic mice. This increase is significantly attenuated in TFPI^{SM22} hypoxic mice (*$P < 0.001$ compared with WT normoxic mice; †$P < 0.001$ compared with WT hypoxic mice, and ‡$P < 0.001$ compared with TFPI^{SM22} normoxic mice; n = 4–6 animals per group). (*D*) Cardiac output is significantly decreased in WT hypoxic mice compared with WT normoxic mice and is maintained in TFPI^{SM22} normoxic or TFPI^{SM22} hypoxic mice (*$P < 0.01$ compared with WT normoxic mice and †$P < 0.01$ compared with WT hypoxic mice; n = 4–6 animals per group). (*E*) Right ventricular ejection fraction is significantly reduced in WT hypoxic mice, whereas no significant change is observed in TFPI^{SM22} normoxic or TFPI^{SM22} hypoxic mice compared with WT normoxic mice (*$P < 0.001$ versus WT normoxic mice and †$P < 0.01$ compared with WT hypoxic mice; n = 4–6 animals per group).

significantly reduced from 12.8 ± 1.8% in WT hypoxic mice to 9.2 ± 0.8% in TFPI^{SM22} hypoxic mice ($P < 0.05$).

Overexpression of TFPI Limits Hypoxia-Induced Fibrin Deposition

To determine whether the beneficial effects of TFPI overexpression are related to its anticoagulant properties, we examined pulmonary fibrin deposition after the initiation of hypoxia (Figures 5A and 5B). Fibrin was nearly absent in lung tissue of WT (WT Day 0) and TFPI^{SM22} (TFPI^{SM22} Day 0) normoxic mice. Fibrin deposition was significantly increased in WT and TFPI^{SM22} mice after 3 and 7 days of hypoxia. After 3 days of hypoxia, fibrin deposition was significantly higher in WT (WT Day 3) mice than in TFPI^{SM22} (TFPI^{SM22} Day 3) mice ($P < 0.001$). No differences in fibrin deposition between WT (WT Day 7) and TFPI^{SM22} (TFPI^{SM22} Day 7) mice were observed after 7 days of hypoxia. These data suggest that hypoxia induces pulmonary fibrin deposition and that overexpression of TFPI limits this process. To confirm that the fibrin deposition that occurs after 3 days of hypoxia is primarily intravascular in nature, we examined lung sections immunofluorescently stained for fibrinogen and vWF. Fibrinous networks colocalized with vWF primarily in the lumen of pulmonary vessels (Figure 5C).

Effects of Chronic Hypoxia on Circulating TF and TFPI Activities

We investigated whether decreased circulating TFPI or increased circulating TF activities contribute to hypoxia-induced fibrin deposition and whether differences between these activities in TFPI^{SM22} and WT mice could explain the differences in fibrin deposition observed. To do so, we measured plasma TF and TFPI activity levels. Circulating TF levels did not change across all four groups of mice (Figure 6A). Furthermore, as

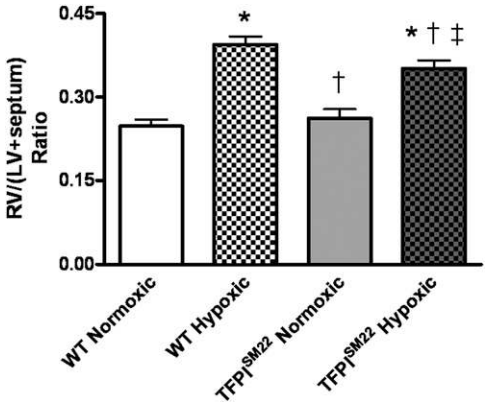

Figure 4. Effect of TFPI overexpression on right ventricular hypertrophy in hypoxia-induced pulmonary arterial hypertension. Ratios of right ventricle (RV) to left ventricle (LV) plus septum (RV/LV+septum) were used as an indicator of RV hypertrophy. Mean ± SEM are shown from 16 or 17 animals per group. Chronic hypoxia induces significant RV hypertrophy in WT and TFPI^{SM22} mice (*$P < 0.001$ compared with WT normoxic mice, †$P < 0.05$ compared with WT hypoxic mice, and ‡$P < 0.001$ compared with TFPI^{SM22} normoxic mice). The extent of hypoxia-induced right ventricular hypertrophy is significantly reduced in the TFPI^{SM22} mice compared with WT mice.

previously reported (35), TFPI^{SM22} mice do not have elevated levels of TFPI activity compared with WT mice under normoxic conditions (Figure 6B). However, in response to hypoxia, there was a significant decrease in plasma TFPI activity observed in the WT and TFPI^{SM22} hypoxic mice when compared with WT and TFPI^{SM22} normoxic mice (Figure 6B). This suggests that the down-regulation of circulating TFPI may be a result of chronic hypoxia, which may contribute to hypoxia-induced fibrin deposition. This finding also suggests that the attenuated increase in fibrin deposition observed in TFPI^{SM22} mice compared with WT mice after 3 days of hypoxia is not due to changes in circulating TFPI or TF activity levels.

Heparin-Releasable TFPI

Because circulating TFPI activity levels cannot explain the differences in fibrin deposition between WT and TFPI^{SM22} mice, we examined the possibility that smooth muscle overexpression of TFPI results in an increased endothelial associated pool of TFPI. To explore this possibility, we used the fact that there is an endothelial pool of TFPI bound to the endothelial surface via heparin sulfate proteoglycans that is released in response to heparin administration (40, 41). Heparin administration (100 U per mouse) resulted in a time-dependent increase in circulating TFPI in WT and TFPI^{SM22} mice as measured by ELISA (Figure 7). At 60 minutes after heparin administration, the TFPI antigen released by heparin administration was significantly higher in the TFPI^{SM22} mice compared with WT mice. This finding suggests that smooth muscle–derived TFPI is secreted and translocated by an unknown mechanism to the endothelial surface, thereby contributing to the endothelial surface–associated (heparin-releasable) pool of TFPI. This finding offers an explanation as to how smooth muscle overexpression of TFPI could affect the intravascular pulmonary fibrin deposition observed in this model.

Overexpression of TFPI Inhibits Vascular Cell Proliferation

Pulmonary vascular hypertrophy and hyperplasia are associated with the pathogenesis of PH. We examined the effects of TFPI overexpression on pulmonary vascular cell proliferation after the initiation of hypoxia (Figure 8A). Two indices of proliferation were examined: one for all vascular cells (total cell proliferation index) and the other specifically for vascular SMCs (SMC proliferation index). Neither the total cell proliferation index ([total PCNA positive nuclei]/[total nuclei]) nor the SMC proliferation index ([PCNA-positive SMC]/[total SMC]) of pulmonary arterioles were significantly different between WT (WT Day 0) and TFPI^{SM22} (TFPI^{SM22} Day 0) mice maintained under normoxic conditions (Figures 8B and 8C). However, 3 days of hypoxia resulted in significant increases in both indexes of proliferation in WT (WT Day 3) and TFPI^{SM22} (TFPI^{SM22} Day 3) mice, although this increase was significantly attenuated in TFPI^{SM22} mice (Figures 8A and 8B). After 7 days of hypoxia, both indexes of proliferation were significantly reduced from those observed after 3 days of hypoxia in WT (WT 7) and TFPI^{SM22} (TFPI^{SM22} 7) mice (Figures 8A and 8B). These results indicate that hypoxia induces pulmonary vascular cell proliferation and that TFPI limits this process.

Because this model approach of TFPI overexpression uses a SMC-specific expression system, we investigated whether this system includes autocrine effects of TFPI on vascular SMC proliferation. To do so, we examined the proliferation of vascular SMCs isolated from WT or TFPI^{SM22} mice. We determined that the TFPI-myc transgene was expressed in SMCs isolated from TFPI^{SM22} mice and absent in cells from WT mice by RT-PCR analysis (data not shown). Transgene-driven overexpression of TFPI resulted in a significant inhibition of vascular SMC proliferation (28%) as determined by BrdU incorporation (Figure 8D; $P < 0.0001$). Thus, in this model system, overexpression of TFPI may have additional autocrine effects on vascular remodeling.

DISCUSSION

Murine models of human disease allow for the use of genetically modified mice. Although inherent limitations exist in rodent models of pulmonary hypertension, the present study used

TABLE 1. PULMONARY VASCULAR REMODELING IN MICE EXPOSED TO CHRONIC HYPOXIA

	WT Normoxia	WT Hypoxia	TFPI^{SM22} Normoxia	TFPI^{SM22} Hypoxia
Vessels counted	79 ± 14	71 ± 17	64 ± 11	83 ± 9
% Muscular*	2.23 ± 0.7	12.8 ± 1.8†	2.02 ± 1.1	9.21 ± 0.8†‡
% Muscular or partly muscular	4.31 ± 1.9	21.3 ± 4.9†	4.10 ± 3.0	17.02 ± 1.3†§

Definition of abbreviations: TFPI^{SM22} = mice that overexpress tissue factor pathway inhibitor via the smooth muscle–specific promoter SM22; WT = wild type.

* % Muscular indicates the percentage of vessels counted that were completely muscularized. % Muscular or partly muscular indicates the percentage of vessels counted that were completely muscularized or partially muscularized.

† $P < 0.05$ versus WT normoxia group (n = 5–6 animals per group).

‡ $P < 0.05$ versus WT hypoxia group (n = 5–6 animals per group).

§ $P = 0.082$ versus WT hypoxia group (n = 5–6 animals per group).

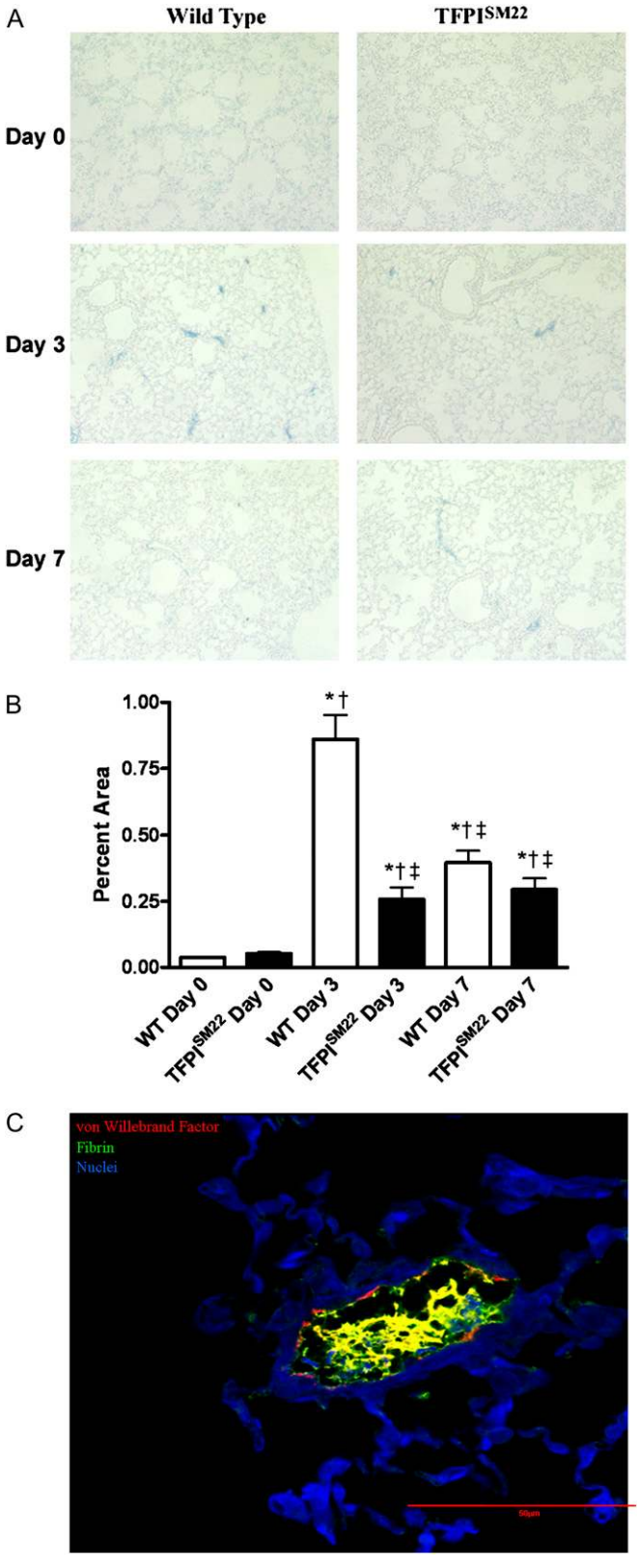

Figure 5. Pulmonary fibrin deposition. Fibrin deposition in the lungs of mice was examined by immunohistochemistry. (*A*) Representative images (original magnification: ×100). (*B*) Fibrin staining was quantified, and the mean ± SEM is summarized using 20 high-power fields per section from three animals per group and is reported as percentage of fibrin staining per total area (*$P < 0.05$ compared with WT Day 0, †$P < 0.05$ compared with TFPI^{SM22} Day 0, and ‡$P < 0.001$ compared with WT Day 3). Staining was nearly absent in normoxic mice (Day 0) and is significantly increased in mice exposed to hypoxia for 3 or 7 days. After 3 days of hypoxia, there was significantly more fibrin deposition in the WT mice compared with the TFPI^{SM22} mice. Fibrin deposition in the WT mice at 3 days returned to levels observed in the TFPI^{SM22} mice at 3 and 7 days. The fibrin staining did not change in the TFPI^{SM22} mice between Days 3 and 7. (*C*) A high-resolution confocal microscopic image of a lung section from a WT 3-day hypoxic mouse immunofluorescently stained for von Willebrand factor (*red*) and fibrin (*green*) demonstrating that fibrin deposition is intravascular. Notice that this vessel is severely occluded.

a chronic hypoxia model based on the important etiologic role of hypoxia in secondary forms of PH. To determine the role of the TF pathway in this model, a transgenic mouse in which TFPI is overexpressed from vascular SMCs was used (TFPI^{SM22}). In these mice, pulmonary TFPI expression is elevated without alterations in circulating TFPI activity levels or changes in TF expression. Chronic hypoxic exposure in WT mice resulted in an increase in right ventricular and pulmonary arterial pressures, increased pulmonary intravascular fibrin deposition, pulmonary vascular remodeling, and RV hypertrophy and decreased cardiac output. Each of these deleterious changes was attenuated in the transgenic mice in which TFPI was overexpressed. Furthermore, hypoxia-induced pulmonary vascular cell proliferation was significantly attenuated in TFPI^{SM22} mice *in vivo*, and an autocrine effect of TFPI overexpression on vascular SMC proliferation was demonstrated *in vitro*. The results from these studies clearly demonstrate beneficial effects of TFPI overexpression on the development and progression of hypoxia-induced PH as measured by changes in hemodynamic parameters and pulmonary vascular remodeling. The results support multiple lines of evidence in humans and other rodent models that suggest that vascular thrombosis plays an integral role in the pathogenesis of pulmonary hypertension (42–45). Because TF and the TF pathway are key components of thrombus formation, inhibition of the extrinsic coagulation cascade by TFPI may be a novel therapeutic approach for the treatment of PH and other prothrombotic disorders.

Although the elevation in right ventricular and pulmonary arterial pressures in response to hypoxia and the improvements in these parameters observed in TFPI^{SM22} mice might be considered modest, important secondary effects of elevated pressures were noted. First, right ventricular hypertrophy, as measured by the RV to LV and septum weight ratios, was evident in WT hypoxic and TFPI^{SM22} hypoxic mice when compared with their normoxic counterparts, and this hypertrophy was reduced in the TFPI^{SM22} mice. Second, diminished cardiac function, as measured by cardiac output and right ventricular ejection fraction, was evident in WT hypoxic mice but not in TFPI^{SM22} mice. This suggests that the magnitude of elevation (in response to hypoxia) and the magnitude of attenuation due to TFPI overexpression resulted in significant improvement in cardiac structure and function in TFPI^{SM22} mice. Although we did not investigate the potential direct effects of TF signaling on cardiac structure or function in the present report, studies by other investigators have suggested that TF expression by cardiomyocytes has an important role in the maintenance of cardiac hemostasis in health and disease (46–48). In a review detailing the role of the TF-thrombin pathway in cardiac ischemia-reperfusion injury, Mackman reported that anti-TF therapy reduces a number of detrimental parameters associated with ischemia-reperfusion injury (46). Although the precise mechanism for these effects has not been established, it appears to be

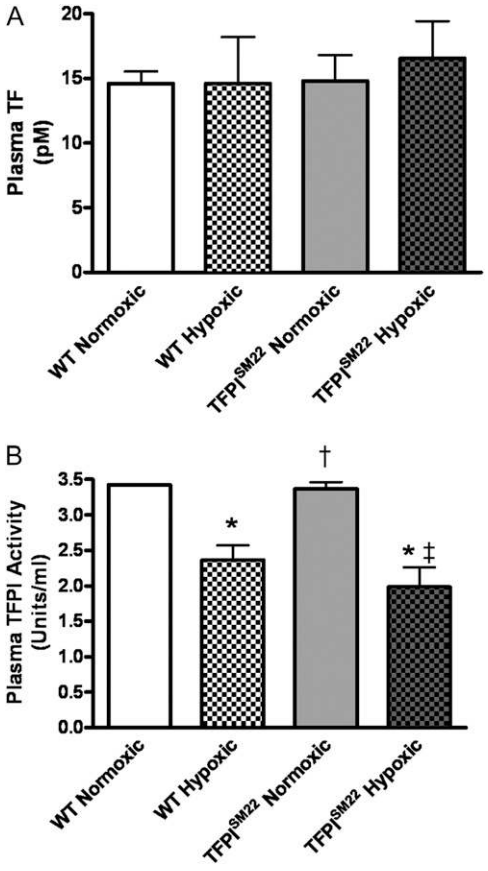

Figure 6. Effects of chronic hypoxia on circulating TF and TFPI activities. TF and TFPI activities were measured in plasma via chromogenic assays. (*A*) Circulating TF levels. No differences in TF activity were observed between all groups of mice ($n = 4$ mice per group). (*B*) Circulating TFPI levels. Plasma TFPI activity was significantly decreased in WT and TFPI^{SM22} hypoxic mice when compared with WT and TFPI^{SM22} normoxic mice (*$P < 0.01$ compared with WT normoxic mice, †$P < 0.05$ compared with WT hypoxic mice, and ‡$P < 0.001$ compared with TFPI^{SM22} normoxic mice; $n = 4$ mice per group).

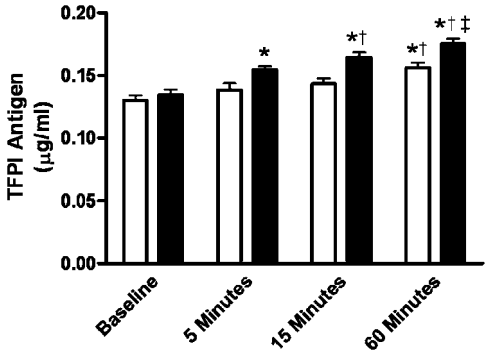

Figure 7. Effects of TFPI overexpression on the heparin-releasable pool of TFPI. TFPI antigen levels were measured by ELISA in plasma of WT (*open bars*) or TFPI^{SM22} (*solid bars*) mice administered 100U heparin or saline ($n = 6$ mice per group). Plasma samples were collected at 0 (Baseline), 5, 15, or 60 minutes. Heparin administration resulted in increased TFPI antigen levels in WT and TFPI^{SM22} mice. However, TFPI antigen levels were higher in the TFPI^{SM22} mice, suggesting an increased heparin-releasable pool (*$P < 0.05$ compared with WT mice at baseline, †$P < 0.001$ compared with TFPI^{SM22} mice at baseline, and ‡$P < 0.05$ compared with WT mice at 60 minutes).

independent of fibrin deposition, and it is suggested that it may involve the activation of protease-activated receptor 1 (PAR-1), also known as the thrombin receptor, present on vascular endothelial cells and cardiomyocytes. The hypothesis for this mechanism is that anti-TF therapy would inhibit thrombin-dependent PAR-1 signaling. Of potential interest to the present studies, Pawlinski and colleagues demonstrated that PAR-1 contributes to the cardiac remodeling and hypertrophy in a murine model of ischemia-reperfusion injury (47). PAR-1 overexpression induces left ventricular eccentric hypertrophy and dilated cardiomyopathy, and cardiomyocyte-specific deletion of TF attenuated the hypertrophy. The authors conclude that inhibition of PAR-1 signaling may represent a novel therapy for heart failure in humans. Although we did not directly address possible TF effects on RV remodeling in the present studies, we may hypothesize that TFPI overexpression could reduce RV hypertrophy via a similar mechanism to the studies detailed above.

Previous studies have shown that chronic hypoxia in mice results in increased pulmonary expression of TF and that this increase is associated with enhanced fibrin deposition and hypoxic induction of intravascular thrombosis (31, 34). The authors of these studies conclude that enhanced expression of TF is the result of the rapid hypoxia-driven induction of EGR-1 and that a likely cellular source for the increased TF is mononuclear phagocytes recruited to the pulmonary bed. We therefore examined fibrin deposition in the lungs of mice exposed to hypoxia. There was increased fibrin deposition after 3 days of hypoxia in WT and TFPI^{SM22} mice compared with mice housed under normoxic conditions. This deposition was significantly reduced in TFPI^{SM22} mice. After 7 days of hypoxia, WT and TFPI^{SM22} mice had fibrin deposition that remained significantly elevated compared with their normoxic counterparts. The deposition observed in WT mice after 3 days of hypoxia was significantly diminished by Day 7 to levels that were observed in TFPI^{SM22} mice at 3 days. These data suggest that in the early stages of hypoxia (3 d), fibrin deposition, and coagulation are favored over fibrinolysis and that overexpression of pulmonary TFPI in the TFPI^{SM22} mice results in a reduction in fibrin deposition when compared with WT mice. This difference is not apparent at 7 days, suggesting a complex regulation between fibrinogenic and fibrinolytic pathways not solely regulated through TFPI expression.

Data from the current studies and from previous studies suggest that in the acute stages of hypoxia there is a transient inflammatory response notable for the infiltration of pulmonary monocytes and tissue factor production (31, 34). We also believe that it is this early fibrin deposition, triggered by the tissue factor pathway (inhibited in the TFPI^{SM22} mice), that initiates the pulmonary vascular remodeling observed with the subsequent development of pulmonary hypertension in this model. Nakamura and colleagues previously reported that TFPI had antiinflammatory effects in a rabbit model of arterial injury (49). In this study, not only did the authors confirm findings of other studies that TFPI inhibited neointimal formation in this model but they also showed that the number of macrophages present at the site of injury was significantly reduced in the TFPI-treated animals. The authors concluded that local delivery of TFPI attenuated neointimal formation via antiinflammatory and antiproliferative effects in addition to, or rather than, antithrombotic effects. In the current studies, we did not investigate the effects of TFPI overexpression on inflammation; however, we cannot rule out the possibility that antiinflammatory effects of TFPI may contribute to the reduced pulmonary vascular remodeling observed in TFPI^{SM22} mice.

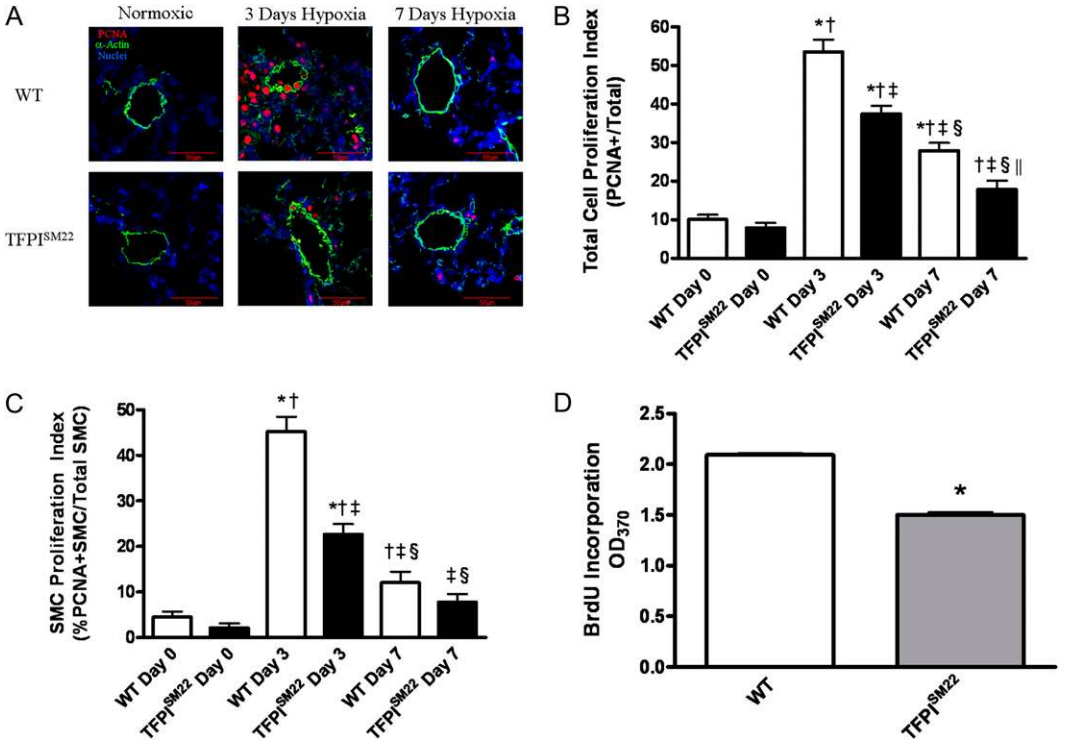

Figure 8. Effects of TFPI overexpression on pulmonary vascular cell proliferation. (*A*) Representative images of lung sections using immunofluoresence staining and confocal microscopy for proliferating cell nuclear antigen (PCNA) (*red*) or α-actin (*green*). Nuclei were visualized by Hoechst staining (*blue*). There is little if any staining for PCNA in sections from WT and TFPI^{SM22} normoxic mice, suggesting the relative absence of vascular proliferation under normoxic conditions. After 3 days of hypoxia, there is a significant increase in the number of cells staining positive for PCNA in WT and TFPI^{SM22} mice, which appears to subside after 7 days of hypoxia. Proliferation was quantified using (*B*) a total cell proliferation index ([total PCNA positive vascular cells]/[total vascular cells]) and (*C*) a vascular smooth muscle cell (SMC) proliferation index ([PCNA-positive vascular SMCs]/[total vascular SMCs]). After 3 days of hypoxia, there is a significant increase in total cell and SMC proliferation indexes in WT and TFPI^{SM22} mice. However, the increases in both indexes are significantly attenuated in TFPI^{SM22} mice after 3 days of hypoxia compared with their WT counterparts. After 7 days of hypoxia, both indexes of proliferation are reduced from the 3-day hypoxia levels. Cells from 15 vessels (20–(100 μm) per animal with three animals per group were analyzed (*$P < 0.001$ compared with WT mice at Day 0, †$P < 0.001$ compared with TFPI^{SM22} mice at Day 0, ‡$P < 0.001$ compared with WT mice Day 3, §$P < 0.05$ compared with TFPI^{SM22} mice at Day, 3 and §$P < 0.05$ compared with WT mice at Day7). (*D*) Effect of TFPI overexpression on vascular SMC proliferation (BrdU incorporation) was examined *in vitro*. Vascular SMCs isolated from the aortas of TFPI^{SM22} mice showed significantly reduced proliferation compared with cells isolated from WT mice (*$P < 0.0001$).

Previous studies have demonstrated a role for TFPI in vascular remodeling. Our laboratory has demonstrated that adenoviral delivery of TFPI resulted in reduced neointimal formation in a flow cessation model of vascular remodeling (50). In another study, mice bred to have a 50% deficiency of functional TFPI showed enhanced neointimal proliferation in a carotid artery ligation model of vascular remodeling (51). TFPI has also been shown to decrease vascular smooth muscle migration and proliferation (21, 22) and to decrease endothelial cell proliferation (23).

Pulmonary vascular remodeling is an important feature of clinical and experimental PH. Hypoxia induces TF production and intravascular fibrin deposition primarily via recruitment of monocytes to the pulmonary bed (31, 34). To our knowledge, the effects of this enhanced TF production on pulmonary vascular remodeling in the chronic hypoxia-induced murine model of PH has not been reported. TF has been shown to induce vascular SMC proliferation and migration via nonhemostatic mechanisms (15, 16). Evidence suggests that TF binding of activated Factor VII (FVIIa) triggers vascular SMC proliferation and that it occurs via extracellular signal-regulated kinase 1 and 2 (ERK 1/2) signaling (15). Camerer and colleagues reported that coexpression of TF, the cellular cofactor for FVIIa, together with PAR-1, PAR-2, PAR-3, or PAR-4, conferred TF-dependent FVIIa activation of PAR-2 and, to lesser degree, PAR-1 (52). Ahamed and colleagues reported that TFPI efficiently inhibits TF-induced ERK 1/2 signaling mediated through PAR2 and to a lesser degree TF-induced PAR-1 signaling responses (53). TFPI-mediated inhibition of TF-mediated PAR-2 signaling may represent a potential mechanism for inhibition of pulmonary vascular cell proliferation contributing to the reduced pulmonary vascular remodeling observed in TFPI^{SM22} mice in this model.

The data presented here suggest that overexpression of TFPI in the current model affected vascular remodeling in two ways: (*1*) the anticoagulant effect of TFPI limits fibrin deposition, which attenuates the procoagulant milieu and matrix in which smooth muscle proliferation is enhanced, and (*2*) TFPI, via its antimitogenic properties, acts locally in an autocrine or paracrine fashion to directly reduce hypoxia-induced pulmonary vascular cell proliferation. In the current studies, we have shown that TFPI overexpression reduces hypoxia-induced fibrin deposition and hypoxia-induced pulmonary vascular cell proliferation *in vivo*. We also demonstrated that TFPI overexpression decreases vascular SMC proliferation *in vitro*. These data suggest that this reduction in proliferative capacity contributes to the decrease in muscularization and vascular cell proliferation observed in the TFPI^{SM22} hypoxic mice compared with WT hypoxic mice and adds to the beneficial effects of TFPI overexpression observed in the TFPI^{SM22} mice.

In conclusion, our data demonstrate that TFPI overexpression results in the attenuation of many of the detrimental changes observed in a hypoxia-induced murine model of PH. Although TF and the TF pathway have been implicated in human and experimental models of PH, this is the first evidence to suggest that TFPI, the endogenous inhibitor of TF, plays

a protective role in hypoxia-induced PH. Therefore, inhibition of the TF pathway may be a novel therapeutic strategy in the treatment of PH associated with hypoxic lung disease.

Conflict of Interest Statement: None of the authors has a financial relationship with a commercial entity that has an interest in the subject of this manuscript.

References

1. Girgis RE, Mathai SC. Pulmonary hypertension associated with chronic respiratory disease. *Clin Chest Med* 2007;28:219–232.
2. Simonneau G, Galie N, Rubin LJ, Langleben D, Seeger W, Domenighetti G, Gibbs S, Lebrec D, Speich R, Beghetti M, *et al.* Clinical classification of pulmonary hypertension. *J Am Coll Cardiol* 2004;43(Suppl S) 5S–12S.
3. Cooper R, Ghali J, Simmons BE, Castaner A. Elevated pulmonary artery pressure: an independent predictor of mortality. *Chest* 1991;99: 112–120. (see comment).
4. Weitzenblum E, Hirth C, Ducolone A, Mirhom R, Rasaholinjanahary J, Ehrhart M. Prognostic value of pulmonary artery pressure in chronic obstructive pulmonary disease. *Thorax* 1981;36:752–758.
5. Barbera JA, Peinado VI, Santos S. Pulmonary hypertension in chronic obstructive pulmonary disease. *Eur Respir J* 2003;21:892–905.
6. Incalzi RA, Fuso L, De Rosa M, Di Napoli A, Basso S, Pagliari G, Pistelli R. Electrocardiographic signs of chronic cor pulmonale: a negative prognostic finding in chronic obstructive pulmonary disease. *Circulation* 1999;99:1600–1605. (see comment).
7. Voelkel NF, Cool CD. Pulmonary vascular involvement in chronic obstructive pulmonary disease. *Eur Respir J Suppl* 2003;46:28s–32s.
8. Presberg KW, Dincer HE. Pathophysiology of pulmonary hypertension due to lung disease. *Curr Opin Pulm Med* 2003;9:131–138.
9. Stenmark KR, Mecham RP. Cellular and molecular mechanisms of pulmonary vascular remodeling. *Annu Rev Physiol* 1997;59:89–144.
10. Howell K, Ooi H, Preston R, McLoughlin P. Structural basis of hypoxic pulmonary hypertension: the modifying effect of chronic hypercapnia. *Exp Physiol* 2004;89:66–72.
11. Hayashida K, Fujita J, Miyake Y, Kawada H, Ando K, Ogawa S, Fukuda K. Bone marrow-derived cells contribute to pulmonary vascular remodeling in hypoxia-induced pulmonary hypertension. *Chest* 2005;127:1793–1798.
12. Stenmark KR, Fagan KA, Frid MG. Hypoxia-induced pulmonary vascular remodeling: cellular and molecular mechanisms. *Circ Res* 2006;99:675–691.
13. Pak O, Aldashev A, Welsh D, Peacock A. The effects of hypoxia on the cells of the pulmonary vasculature. *Eur Respir J* 2007;30:364–372.
14. Wagenvoort CA. Classifying pulmonary vascular disease. *Chest* 1973;64: 503–504.
15. Cirillo P, Cali G, Golino P, Calabro P, Forte L, De Rosa S, Pacileo M, Ragni M, Scopacasa F, Nitsch L, *et al.* Tissue factor binding of activated factor vii triggers smooth muscle cell proliferation via extracellular signal-regulated kinase activation. *Circulation* 2004;109: 2911–2916.
16. Sato Y, Asada Y, Marutsuka K, Hatakeyama K, Sumiyoshi A. Tissue factor induces migration of cultured aortic smooth muscle cells. *Thromb Haemost* 1996;75:389–392.
17. Broze GJ Jr. The role of tissue factor pathway inhibitor in a revised coagulation cascade. *Semin Hematol* 1992;29:159–169.
18. Broze GJ Jr. Tissue factor pathway inhibitor and the revised theory of coagulation. *Annu Rev Med* 1995;46:103–112.
19. Broze GJ Jr. Tissue factor pathway inhibitor and the current concept of blood coagulation. *Blood Coagul Fibrinolysis* 1995;6:S7–S13.
20. Girard TJ, Broze GJ Jr. Tissue factor pathway inhibitor. *Methods Enzymol* 1993;222:195–209.
21. Kamikubo Y, Nakahara Y, Takemoto S, Hamuro T, Miyamoto S, Funatsu A. Human recombinant tissue-factor pathway inhibitor prevents the proliferation of cultured human neonatal aortic smooth muscle cells. *FEBS Lett* 1997;407:116–120.
22. Sato Y, Asada Y, Marutsuka K, Hatakeyama K, Kamikubo Y, Sumiyoshi A. Tissue factor pathway inhibitor inhibits aortic smooth muscle cell migration induced by tissue factor/factor viia complex. *Thromb Haemost* 1997;78:1138–1141.
23. Hembrough TA, Ruiz JF, Papathanassiu AE, Green SJ, Strickland DK. Tissue factor pathway inhibitor inhibits endothelial cell proliferation via association with the very low density lipoprotein receptor. *J Biol Chem* 2001;276:12241–12248.
24. Herve P, Humbert M, Sitbon O, Parent F, Nunes H, Legal C, Garcia G, Simonneau G. Pathobiology of pulmonary hypertension: the role of platelets and thrombosis. *Clin Chest Med* 2001;22:451–458.
25. Dartevelle P, Fadel E, Mussot S, Chapelier A, Herve P, de Perrot M, Cerrina J, Ladurie FL, Lehouerou D, Humbert M, *et al.* Chronic thromboembolic pulmonary hypertension. *Eur Respir J* 2004;23:637–648.
26. Altman R, Scazziota A, Rouvier J, Gurfinkel E, Favaloro R, Perrone S, Fareed J. Coagulation and fibrinolytic parameters in patients with pulmonary hypertension. *Clin Cardiol* 1996;19:549–554.
27. Bakouboula B, Morel O, Faure A, Zobairi F, Jesel L, Trinh A, Zupan M, Canuet M, Grunebaum L, Brunette A, *et al.* Procoagulant membrane microparticles correlate with the severity of pulmonary arterial hypertension. *Am J Respir Crit Care Med* 2008;177:536–543.
28. White RJ, Meoli DF, Swarthout RF, Kallop DY, Galaria II, Harvey JL, Miller CM, Blaxall BC, Hall CM, Pierce RA, *et al.* Plexiform-like lesions and increased tissue factor expression in a rat model of severe pulmonary arterial hypertension. *Am J Physiol Lung Cell Mol Physiol* 2007;293:L583–L590.
29. White RJ, Galaria II, Harvey J, Blaxall BC, Cool CD, Taubman MB. Tissue factor is induced in a rodent model of severe pulmonary hypertension characterized by neointimal lesions typical of human disease. *Chest* 2005;128(Suppl):612S–613S.
30. Campian ME, Hardziyenka M, Michel MC, Tan HL. How valid are animal models to evaluate treatments for pulmonary hypertension? *Naunyn Schmiedebergs Arch Pharmacol* 2006;373:391–400.
31. Yan SF, Zou YS, Gao Y, Zhai C, Mackman N, Lee SL, Milbrandt J, Pinsky D, Kisiel W, Stern D. Tissue factor transcription driven by egr-1 is a critical mechanism of murine pulmonary fibrin deposition in hypoxia. *Proc Natl Acad Sci USA* 1998;95:8298–8303.
32. Yan SF, Mackman N, Kisiel W, Stern DM, Pinsky DJ. Hypoxia/hypoxemia-induced activation of the procoagulant pathways and the pathogenesis of ischemia-associated thrombosis. *Arterioscler Thromb Vasc Biol* 1999;19:2029–2035.
33. Yan SF, Pinsky DJ, Stern DM. A pathway leading to hypoxia-induced vascular fibrin deposition. *Semin Thromb Hemost* 2000; 26:479–483.
34. Lawson CA, Yan SD, Yan SF, Liao H, Zhou YS, Sobel J, Kisiel W, Stern DM, Pinsky DJ. Monocytes and tissue factor promote thrombosis in a murine model of oxygen deprivation. *J Clin Invest* 1997;99: 1729–1738.
35. Pan S, Kleppe LS, Witt TA, Mueske CS, Simari RD. The effect of vascular smooth muscle cell-targeted expression of tissue factor pathway inhibitor in a murine model of arterial thrombosis. *Thromb Haemost* 2004;92:495–502.
36. Champion HC, Bivalacqua TJ, Toyoda K, Heistad DD, Hyman AL, Kadowitz PJ. In vivo gene transfer of prepro-calcitonin gene-related peptide to the lung attenuates chronic hypoxia-induced pulmonary hypertension in the mouse. *Circulation* 2000;101:923–930. (see comment).
37. Paddenberg R, Stieger P, von Lilien AL, Faulhammer P, Goldenberg A, Tillmanns HH, Kummer W, Braun-Dullaeus RC. Rapamycin attenuates hypoxia-induced pulmonary vascular remodeling and right ventricular hypertrophy in mice. *Respir Res* 2007;8:15.
38. West J, Fagan K, Steudel W, Fouty B, Lane K, Harral J, Hoedt-Miller M, Tada Y, Ozimek J, Tuder R, *et al.* Pulmonary hypertension in transgenic mice expressing a dominant-negative bmprii gene in smooth muscle. *Circ Res* 2004;94:1109–1114.
39. Hales CA, Kradin RL, Brandstetter RD, Zhu YJ. Impairment of hypoxic pulmonary artery remodeling by heparin in mice. *Am Rev Respir Dis* 1983;128:747–751.
40. Novotny WF, Brown SG, Miletich JP, Rader DJ, Broze GJ Jr. Plasma antigen levels of the lipoprotein-associated coagulation inhibitor in patient samples. *Blood* 1991;78:387–393.
41. Sandset PM, Abildgaard U, Larsen ML. Heparin induces release of extrinsic coagulation pathway inhibitor (epi). *Thromb Res* 1988;50: 803–813.
42. Hassell KL. Altered hemostasis in pulmonary hypertension. *Blood Coagul Fibrinolysis* 1998;9:107–117.
43. Bjornsson J, Edwards WD. Primary pulmonary hypertension: a histopathologic study of 80 cases. *Mayo Clin Proc* 1985;60:16–25.
44. Chaouat A, Weitzenblum E, Higenbottam T. The role of thrombosis in severe pulmonary hypertension. *Eur Respir J* 1996;9:356–363.
45. Wagenvoort CA, Mulder PG. Thrombotic lesions in primary plexogenic arteriopathy: similar pathogenesis or complication? *Chest* 1993;103: 844–849. (see comment).

46. Mackman N. The role of the tissue factor-thrombin pathway in cardiac ischemia-reperfusion injury. *Semin Vasc Med* 2003;3:193–198.
47. Pawlinski R, Tencati M, Hampton CR, Shishido T, Bullard TA, Casey LM, Andrade-Gordon P, Kotzsch M, Spring D, Luther T, *et al.* Protease-activated receptor-1 contributes to cardiac remodeling and hypertrophy. *Circulation* 2007;116:2298–2306. (see comment).
48. Pawlinski R, Tencati M, Holscher T, Pedersen B, Voet T, Tilley RE, Marynen P, Mackman N. Role of cardiac myocyte tissue factor in heart hemostasis. *J Thromb Haemost* 2007;5:1693–1700.
49. Nakamura Y, Nakamura K, Ohta K, Matsubara H, Yutani C, Hamuro T, Kato H, Ohe T. Anti-inflammatory effects of long-lasting locally-delivered human recombinant tissue factor pathway inhibitor after balloon angioplasty. *Basic Res Cardiol* 2002;97:198–205.
50. Singh R, Pan S, Mueske CS, Witt T, Kleppe LS, Peterson TE, Slobodova A, Chang JY, Caplice NM, Simari RD. Role for tissue factor pathway in murine model of vascular remodeling. *Circ Res* 2001;89:71–76.
51. Singh R, Pan S, Mueske CS, Witt TA, Kleppe LS, Peterson TE, Caplice NM, Simari RD. Tissue factor pathway inhibitor deficiency enhances neointimal proliferation and formation in a murine model of vascular remodelling. *Thromb Haemost* 2003;89:747–751.
52. Camerer E, Huang W, Coughlin SR. Tissue factor- and factor x-dependent activation of protease-activated receptor 2 by factor viia. *Proc Natl Acad Sci USA* 2000;97:5255–5260.
53. Ahamed J, Belting M, Ruf W. Regulation of tissue factor-induced signaling by endogenous and recombinant tissue factor pathway inhibitor 1. *Blood* 2005;105:2384–2391.